NANO LETTERS

2005
Vol. 5, No. 11
2174−2178

# Surface-Driven Bulk Reorganization of Gold Nanorods

**Yanting Wang,[†] S. Teitel,*[,†] and Christoph Dellago[‡]**

*Department of Physics and Astronomy, University of Rochester, Rochester, New York 14627, and Institute for Experimental Physics, University of Vienna, Boltzmanngasse 5, 1090 Vienna, Austria*

*Received June 17, 2005; Revised Manuscript Received September 28, 2005*

**ABSTRACT**

**Molecular dynamic simulations are used to study the structural stability of gold nanorods upon heating. We show that the global stability of the rod is governed by the free energetics of its surface. In particular, an instability of surface facets nucleates a bulk instability that leads to both surface and bulk reorganization of the rod. The surface reorganizes to form new, more stable, {111} facets, while the underlying fcc lattice completely reorients to align with this new surface structure. Rods with predominantly {111} facets remain stable until melting.**

The global shape of a crystal structure is in general determined by its growth process. For macroscopic-sized crystals, this shape will rarely be the true *equilibrium shape* that minimizes the total free energy; slow diffusion over macroscopic length scales generally result in a bulk structure and nonequilibrium global shape that are stable on all experimental time scales. Metallic crystals of micrometer size, however, have been observed to take their equilibrium shape when annealed for long times at high temperatures.[1] The standard theory of equilibrium shapes[2] minimizes the surface free energy, assuming that the bulk free energy remains constant. Surfaces are assumed to be large enough that the thermodynamic limit applies, and the vanishing of a surface facet is determined by the roughening transition of the corresponding surface. It is generally assumed that the equilibrium shape is achieved by a process of surface diffusion.

For structures on the *nanometer* scale, however, where surface and bulk free energies may be comparable, such a clear division between surface and bulk effects is no longer obvious. Moreover, when surface facets are only several atoms across, it is not clear that they will behave in the same manner as macroscopically large surfaces. Recent calculations by Zhao and Yakobson[3] for silicon nanowires have explicitly decomposed the energy into bulk, surface, and edge contributions, showing the importance of the surface and edge terms in determining the globally stable structure. Diao et al.,[4] in numerical simulations of ⟨100⟩ oriented gold nanowires with small cross-sectional areas ($<4$ nm$^2$), showed that the surface strain associated with {100} facets can drive a transformation of the interior from the fcc structure that is the stable structure for macroscopic bulk gold, to a bct (body-centered tetragonal) structure. It is therefore of great interest to study under what situations nanostructures with nonequilibrium initial shapes may become globally unstable, identify the particular mechanism leading to the instability, and study the resulting kinetic path that the system takes to achieve a more stable shape.

In this work, we consider gold nanorods of low aspect ratio $\sim$3, as have been studied in recent laser heating experiments.[5−8] Using molecular dynamic (MD) simulations of a rod with a few thousand atoms, we find that the stability of the nanorod against changes in shape and bulk structure is still governed by the energetics of its surface facets. A rod covered primarily by {111} facets remains stable up until melting. However, for a rod that has a sizable fraction of its surface covered by {110} or {100} facets, an instability of those facets sets in well below melting and leads to a shape transformation to a shorter and wider structure. The surface reorganizes to form higher stability {111} facets. More surprisingly, the fcc interior completely reorganizes as well, rotating to align with the new facet planes.

The initial rod configuration that we consider, shown in Figure 1, is that proposed in ref 5. The interior of the rod is a pure fcc lattice. The surface of the rod consists of four large {100} and four large {110} facets oriented parallel to the rod axis. The ends of the rod have a {001} facet and four small {111} facets connecting the {110} and the {001} facets. These experiments found that, upon heating, such rods underwent a shape transformation to bent, twisted, shorter, wider, and "$\phi$-shaped" rods in which the middle of the rod bulges outward. Transmission electron miscroscopy studies[8] observed point and planar internal defects to accompany such

* Corresponding author. E-mail: stte@pas.rochester.edu.
[†] University of Rochester.
[‡] University of Vienna.

10.1021/nl051149h CCC: $30.25 
**Published on Web 10/20/2005**

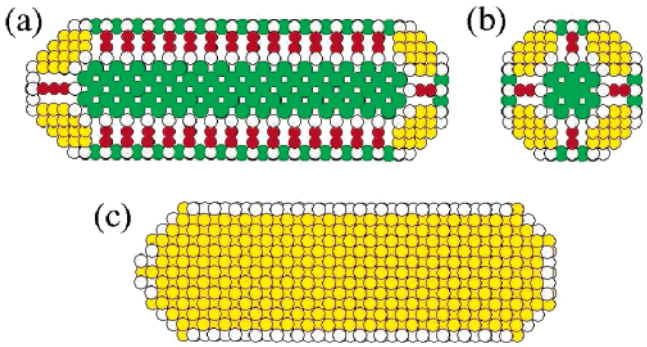


**Figure 1.** Initial configuration of the gold nanorod with $N = 2624$ atoms and aspect ratio 3: (a) side view, (b) end view down the long axis, (c) cross-sectional view parallel to long axis. In a and b, yellow atoms represent {111} facets, green atoms represent {100} facets, and red atoms represent {110} facets; white atoms are on the edges. In c, yellow atoms are those with a local fcc structure, white atoms are on the surface; the cross-sectional view in c shows atoms in the square arrangement of a {100} plane of the fcc lattice.

shape transformations. Recent MD simulations[9] of such rods, using a continuous heating procedure meant to model the laser heating of experiments, found similar shape transformations. These simulations found the shape transformation to be accompanied by a structural change in which planes of interior atoms shift, converting local fcc structure to hcp. The extent and stability of these interior rearrangements was found to depend on both the heating rate and the number of atoms in the cluster, but no specific mechanism or energetic argument for this structural rearrangement was proposed. In this paper we present new simulations carried out with a much slower "quasiequilibrium" heating that allows the rod more time to approach configurations of local equilibrium. Our results make it clear that it is the energetics of the surface that is driving the shape and structural transformation.

We use the empirical "glue" potential[10] to model the many body interactions of the gold atoms in our simulated nanorod, and we integrate the classical equations of motion for the atoms using the velocity Verlet algorithm[11] with a time step of 4.3 fs. However, instead of increasing the kinetic energy at each MD step to model continuous heating as in ref 9, we now use the Gaussian isokinetic thermostat[12] to keep the total kinetic energy fixed at a constant temperature $T$; after each MD step, all velocities are rescaled by a constant factor so as to keep $\langle(1/2)mv^2\rangle = (3/2)k_BT$ fixed. Our procedure conserves total linear and angular momenta, which are set to zero so that our rod does not drift or rotate throughout our simulation. At each fixed $T$, we carry out $10^7$ MD steps for a simulated time of 43 ns before increasing the temperature in jumps of 100 K. Our effective heating rate is therefore $\sim 2.3 \times 10^9$ K/s, more than 3 orders of magnitude slower than the continuous heating rates of $2-7 \times 10^{12}$ K/s used in ref 9. We use a rod of $N = 2624$ atoms with an initial aspect ratio of 3, as shown in Figure 1. The length of the rod, parallel to its long axis, is 7.38 nm, and its cross-sectional area has a diameter of 2.46 nm. We do a short equilibration for 430 ps ($10^5$ MD steps) at 5 K in order to relax the surface atoms of the rod from their initial fcc positions before starting to heat the rod.

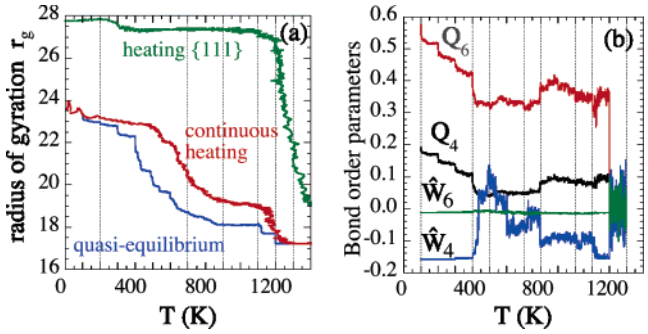


**Figure 2.** (a) Radius of gyration $r_g$ vs temperature $T$ for the rod of Figure 1: quasiequlibrium heating (blue) compared to the continuous heating of ref 9 (red); continuous heating of the rod with structure of Figure 3 (green). (b) Bond order parameters, $Q_4$, $Q_6$, $\hat{W}_4$, and $\hat{W}_6$, averaged over all atoms internal to the rod, vs temperature $T$, for quasiequlibrium heating of the rod of Figure 1.

As a signature of the shape change of our nanocluster, we measure the radius of gyration, $r_g$, defined by $r_g^2 = (1/N)\sum_i|\mathbf{r}_i - \mathbf{r}_c|^2$, where $\mathbf{r}_i$ is the position of atom $i$ and $\mathbf{r}_c$ is the center of mass. In Figure 2a we plot our results for $r_g$ as the system is heated; the blue curve is for our above quasiequilibrium heating. The vertical dotted lines separate bins of constant temperature simulation, where the temperature is equal to the value at the left end point of the bin; the data plotted within each bin represents the instantaneous value of $r_g$ as a function of increasing time at the constant temperature. At the end of each bin, the temperature is increased by a jump of 100 K. We plot our data this way, instead of as an average value at each $T$, to highlight that significant shape relaxation occurs even at constant $T$. For comparison, we plot $r_g$ for the continuous heating (red curve) of ref 9 for the heating rate of $7 \times 10^{12}$ K/s; here the temperature is determined from the instantaneous value of the average kinetic energy. We see that the curves are qualitatively similar, with the onset of a plateau around 800 K; however, the present quasiequilibrium heating allows the rod to relax to smaller $r_g$ values before the rod melts at $T \approx$ 1200 K. The decrease in the radius of gyration reflects the shape transformation to a shorter wider rod of a smaller aspect ratio.

To investigate the local structure within the cluster, we use the method of bond orientational order parameters.[13] These parameters measure the orientation of bonds connecting a given atom to its nearest neighbors and provide a convenient means of determining the local crystalline structure of an atom. In particular, we measure the 6-fold and 4-fold orientation parameters, $Q_6$, $\hat{W}_6$, $Q_4$, and $\hat{W}_4$. We refer the reader to the literature for their definitions,[9,13] and in Table 1 we give their values for several periodic 3D crystal structures. In Table 1, we also give the values of these parameters as computed for atoms on particular low-index planar surfaces of an fcc bulk crystal; for these 2D parameters we average only over bonds connecting an atom with its neighbors in the specified plane. In Figure 2b, we plot these order parameters for our rod, averaging over only atoms internal to the rod (i.e., we exclude surface atoms because these have fewer nearest neighbor bonds). As for $r_g$, we plot our data as the instantaneous value as a function of increasing

**Table 1.** Bond Order Parameters for Face-Centered Cubic (fcc), Hexagonal Close-Packed (hcp), Simple Cubic (sc), Body-Centered Cubic (bcc), and Low-Index fcc Planes

| geometry | $Q_4$ | $Q_6$ | $\hat{W}_4$ | $\hat{W}_6$ |
|---|---|---|---|---|
| fcc | 0.19094 | 0.57452 | −0.15932 | −0.01316 |
| hcp | 0.09722 | 0.48476 | 0.13410 | −0.01244 |
| sc | 0.76376 | 0.35355 | 0.15932 | 0.01316 |
| bcc | 0.08202 | 0.50083 | 0.15932 | 0.01316 |
| {110} | 1 | 1 | 0.13410 | −0.09306 |
| {100} | 0.82916 | 0.58630 | 0.12497 | −0.00721 |
| {111} | 0.37500 | 0.74083 | 0.13410 | −0.04626 |

simulation time, for bins of constant temperature (indicated by the dotted vertical lines). Comparing with Table 1, we see that the rod maintains its fcc structure until about 400 K. Then, from around 400 K to about 800 K, there is a rise to positive values in $\hat{W}_4$ and a decrease in $Q_6$ and $\hat{W}_6$, suggestive of a more hcp-like structure. Above 800 K, the values return to their fcc-like values.

We now focus on the structure of the rod in the high-temperature plateau region where $r_g$ stabilizes to a constant. In Figure 3 we show the configuration of the rod at $T =$ 900 K, in the constant plateau region before melting. The views of the rod shown in Figure 3a−c are the same orientations as shown for the initial configuration in Figure 1a−c. To better illustrate the order of the rod, we first pick an instantaneous configuration sampled from the middle of the $T = 900$ K simulation and use the conjugate gradient method[14] to quench local thermal fluctuations. At such high temperatures, the surface can be partially disordered compared to the interior because of the diffusion of atoms on and near facet edges and vertices.[15,16] We therefore use the *cone algorithm*[16] to identify and peel away atoms on the surface and in the first sublayer below it and in Figure 3a and b show the configuration of the second sublayer of the rod. We see a very regular shape covered almost completely with stable {111} facets. On the basis of the values in Table 1, we use the following criteria to identify atoms in this layer as belonging to particular low-index planes: {111} if $0.7 < Q_6 < 0.9$ and $-0.08 < \hat{W}_6 < -0.02$; {100} if $Q_6 < 0.7$ and $\hat{W}_6 > -0.02$; and {110} if $Q_6 > 0.9$ and $\hat{W}_6 < -0.08$. Atoms in Figure 3a and b have been colored accordingly.

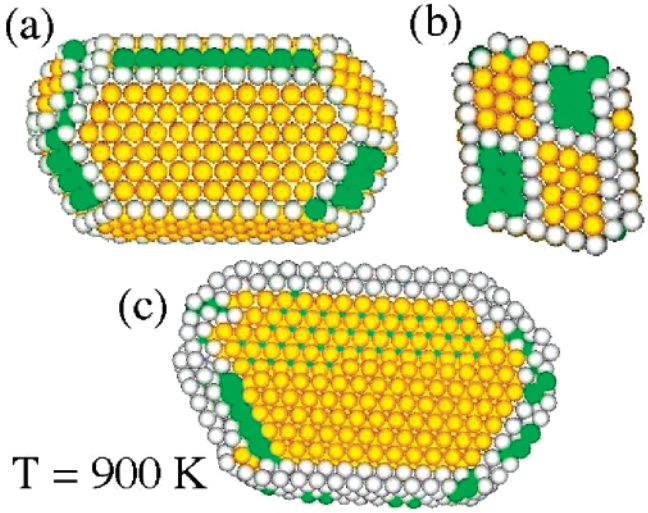


**Figure 3.** Configuration of the nanorod after quasiequilibrium heating to 900 K. (a) side view, and (b) end view down the long axis, after peeling away the surface and the first subsurface layer; yellow atoms are {111} facets, green atoms are {100} facets, and white are edge atoms. (c) Cross-sectional view parallel to the long axis; yellow atoms have a local fcc structure, green atoms have a local hcp structure, and white atoms are neither. The cross-sectional view in c shows atoms in the close-packed hexagonal arrangement of a {111} plane of the fcc lattice.

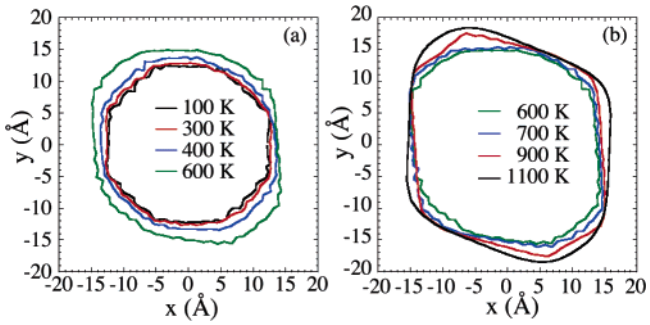


**Figure 4.** Average cross-sectional shape, viewed down the long axis of the rod, for different temperatures.

The cross-sectional view in Figure 3c shows an almost pure fcc interior, as was the case for the initial configuration; however, we now see a close-packed hexagonal structure characteristic of a {111} plane of the fcc lattice, rather than the {100} plane seen in the cross-sectional view of Figure 1c. We thus see one of our main results: in order to align with the new {111} surface facets, the bulk fcc structure has completely reorganized itself to a new orientation. For interior atoms, we use the following criteria to identify the local crystal structure: fcc if $Q_4 > 0.17$ and $\hat{W}_4 < -0.10$; hcp if $Q_4 < 0.13$ and $\hat{W}_4 > 0.07$. Atoms in Figure 3c have been colored accordingly.

To see how the rod evolves from its initial configuration (Figure 1) to its reorganized shape (Figure 3), we consider the average cross-sectional shape in a plane transverse to the long axis of the rod. We compute this average shape as follows: For each instantaneous configuration, we first eliminate all atoms on the end caps of the rods and all interior atoms of the rod and then project the remaining surface atoms into the *xy* plane, perpendicular to the long axis of the rod. Placing the origin at the resulting center of mass, we divide the plane into 100 equal polar angles and then compute the average position of all surface atoms in each angular division. This result is then averaged over 1000 different instantaneous configurations sampled uniformly throughout the simulated time of 43 ns at each temperature, *T*. We plot the resulting average cross-sectional shapes, for several different *T*, in Figure 4.

At low *T* we see the octagonal cross-section of the initially constructed rod of Figure 1, with the flat edges representing the initial {100} and {110} facets. The shape stays roughly the same until about 400 K. Somewhere between 300 and 400 K, the shape becomes rounder and the initial flat edges disappear. As *T* increases further, the cross-sectional area grows, representing the shape transformation to a shorter and wider rod of lower aspect ratio, and we see new flat facets

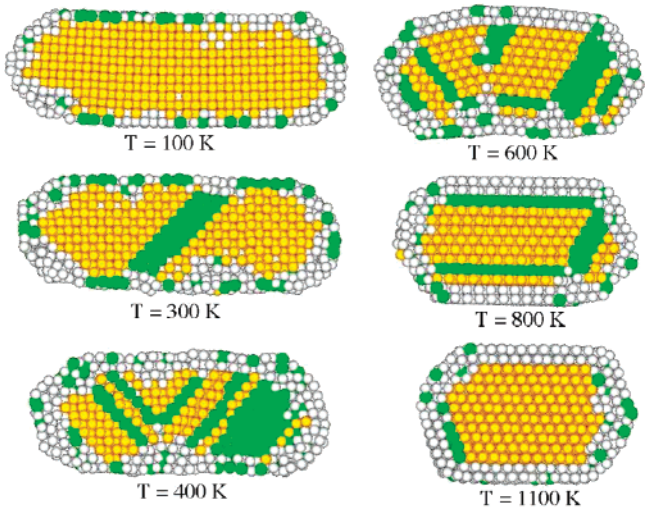


**Figure 5.** Cross-sectional view for various temperatures. Atoms are colored according to local crystal structure: fcc is yellow, hcp is green, neither is white.

develop and grow in new directions. At 900 K we see the fully faceted shape shown in Figure 3.

In a macroscopic sample, the disappearance of flat facets, with the resulting rounding of the average shape, is a signature of the roughening transition of those surfaces.[2] It is known from experiments that the gold {110} surface roughens at 680 K,[17] while the {100} surface disorders at ~1170 K,[18] below the bulk melting temperature of 1337 K. In contrast, the macroscopic {111} surface is believed to remain stable up to, and even above, the bulk melting.[19] The instability that initiates the shape change that we find in our nanorod at 400 K may therefore just correspond to the roughening transition of the {110} facets, which has been shifted to lower temperature because of large finite size effects in our relatively small rod. After this instability, the surface reorganizes to form mostly lower free energy {111} facets, which remain stable until melting. Note that the fully faceted cross-sectional shape at 900 K contains four large sides and two short sides; the former are the {111} facets, while the latter are {100} facets. By 1100 K, these {100} facets have been replaced by a smoothly curved surface. We infer that this is due to the disordering transition of the {100} surface, reduced somewhat in temperature because of finite size effects.

To see how the interior fcc structure of the rod reorganizes itself to a new orientation, we show cross-sectional views of the rod at various temperatures in Figure 5. We color the atoms according to their local crystal structure using the criteria given above: fcc is yellow, hcp is green, neither is white. Initially, the interior is pure fcc, oriented so that the cross-sectional view shows a {100} plane of atoms. As temperature increases, we see that the shape and structural transformation is accompanied by the appearance of hcp planes inside the rod interior because of the sliding of {111} planes. As temperature increases further, the surface becomes less ordered and more {111} planes with different orientations slide. Around 800 K, the surface has reordered and the interior fcc lattice has reoriented so that the cross-sectional view now shows a predominantly {111} plane of atoms. At 1100 K, the interior has completely reordered to pure fcc, but with the new orientation.

Such behavior as described above may well exist in other simple elemental metals. We note that many such metals similarly have a roughening transition, $T_R$, for the {110} surface that is significantly below the bulk melting, $T_m$. Silver, for example, has $T_R = 600$ K and $T_m = 1235$ K, with a similar ratio of $T_R/T_m$ as gold.[21] Lead has $T_R = 415$ K and $T_m = 601$ K, for a somewhat larger $T_R/T_m$ than gold.[22]

Finally, to verify that instability of the particular surface facets, rather than just the minimization of total surface area, is indeed the mechanism for the shape transformation, we study the stability of a gold nanorod with an aspect ratio of ~3, but with an initial structure similar to that of Figure 3 with a surface predominantly covered by {111} facets. We use a continuous heating MD simulation with a heating rate of $7 \times 10^{12}$ K/s to model laser heating experiments for a rod with 3411 atoms. Our results for $r_g$ versus $T$ are shown in Figure 2a (green curve). Unlike the intial rod of Figure 1, we now find that the rod remains stable, with no significant shape or structural rearrangement up until the rod melting temperature. Experiments[23] have shown that nanosized Pb clusters with large {111} surfaces can superheat above melting, consistent with our results. We conclude that the stability of gold, and presumably other metallic nanorods, is crucially dependent upon the structure of the rod surface. Once a shape instability is nucleated, however, the entire bulk of the rod participates in the restructuring.

After our work was completed, we learned of similar work by Diao et al.[24] who carried out finite temperature molecular dynamic simulations of gold nanorods, oriented similarly as our initial configuration of Figure 1, but with a square cross-section and surface covered entirely by {100} facets. Using two different empirical potentials, the "modified embedded atom method" (MEAM) and the "embedded atom method" (EAM) (in contrast to our use of the glue potential), they simulated rods of much larger aspect ratios than those considered here. For the MEAM, they studied a rod of similar cross-sectional area to ours, but for EAM they used a rod with cross-sectional area roughly one-quarter of ours. Despite the different rod shape, aspect ratio, and model potential, they found that at around 300 K the rod transformed to a shape similar to our Figure 3, consisting of a rhomboidal cross-section, a surface covered by {111} facets, and with the fcc interior having rotated to align with the new facets. For the EAM potential, this transformation occurred by a similar mechanism of sliding {111} planes as we have found here. They, however, attribute this transformation to the effects of surface stress on the {100} facets.

To clarify whether it is the {110} or the {100} facets on our initial rod of Figure 1 that are responsible for the transformation we see, we have carried out new simulations for initial rods of roughly the same cross-sectional area and aspect ratio as in Figure 1, but now with a square cross-section oriented so that in one case (a) the length of the rod has only {110} surface facets (this rod has 2546 atoms), and in a second case (b) the length of the rod has only {100}

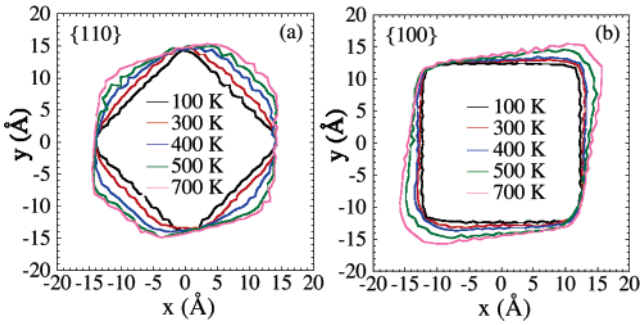


**Figure 6.** Average cross-sectional shape viewed down the long axis of the rod, at different temperatures, for (a) a rod initially covered only by {110} facets, and (b) a rod initially covered by only {100} facets.

surface facets (this rod has 3126 atoms). Heating for a simulated time of 4.3 ns per temperature with temperature jumps of 100 K, and using the glue potential, we find in both cases a transformation at $T \approx 300-400$ K to a structure similar to that in Figure 3, with a rotated fcc interior and surface covered primarily by {111} facets. In Figure 6 we show the average cross-sectional areas at different temperatures, computed by the same method as used earlier in Figure 4, for both of these cases (a and b). For case a of the {110} covered rod, we see the same rounding out of the {110} facets as the rod begins its transformation to its final shape, as we saw in Figure 4. For case b of the {100} covered rod, however, we see no rounding of the facets; rather, the corner edges in the ⟨110⟩ directions round, and the initial {100} facets reorient to {111} while remaining perfectly flat. Inspection of the internal structure of the {100} covered rod shows that an hcp plane appears as early as at $T = 200$ K. By comparing to the results of case a, we conclude that in our original rod of Figure 1, it is the {110} facets that nucleate the shape transformation, possibly because of the roughening transition of these facets. The results we find for the {100} covered rod, however, indicate that more than one mechanism may be important for the transformation of gold nanorods. In all cases, though, the nanorod finds a mechanism to restructure its surface to have stable {111} facets dominating, while the interior atoms of the rod participate in this transformation by a reorientation of their initial fcc structure.

**Acknowledgment.** This work was funded in part by DOE grant DE-FG02-89ER14017.

## References

(1) (a) Heyraud, J. C.; Métois, J. J. *Surf. Sci.* **1983**, *128*, 334. (b) Heyraud, J. C.; Métois, J. J. *J. Cryst. Growth* **1980**, *50*, 571.
(2) Jayaprakash, C.; Saam, W. F.; Teitel, S. *Phys. Rev. Lett.* **1983**, *50*, 2017; and references therein.
(3) Zhao, Y.; Yakobson, B. I. *Phys. Rev. Lett.* **2003**, *91*, 35501.
(4) Diao, J.; Gall, K.; Dunn, M. L. *Nat. Mater.* **2003**, *2*, 656.
(5) Wang, Z. L.; Mohamed, M. B.; Link, S.; El-Sayed, M. A. *Surf. Sci.* **1999**, *440*, L809.
(6) Chang, S.; Shih, C.; Lai, W.; Wang, C. R. C. *Langmuir* **1999**, *103*, 1165.
(7) Link, S.; Burda, C.; Nikoobakht, B.; El-Sayed, M. A. *J. Phys. Chem. B* **2000**, *104*, 6152.
(8) Link, S.; Wang, Z. L.; El-Sayed, M. A. *J. Phys. Chem. B* **2000**, *104*, 7867.
(9) Wang, Y.; Dellago, C. *J. Phys. Chem. B* **2003**, *107*, 9214.
(10) Ercolessi, F.; Parrinello, M.; Tosatti, E. *Philos. Mag. A* **1988**, *58*, 213.
(11) Allen, M. P.; Tildesley, D. J. *Computer Simulation of Liquids*; Clarendon Press: Oxford, 1987.
(12) Evans, D. J.; Hoover, W. G.; Failor, B. H.; Moran, B.; Ladd, A. J. C. *Phys. Rev. A* **1983**, *28*, 1016.
(13) Steinhardt, P. J.; Nelson, D. R.; Ronchetti, M. *Phys. Rev. B* **1983**, *28*, 784.
(14) Press, W. H.; Teukolsky, S. A.; Vetterling, W. T.; Flannery, B. P. *Numerical Recipes in C: The Art of Scientific Computing*; Cambridge University Press: Cambridge, 1992.
(15) Wang, Y.; Teitel, S.; Dellago, C. *Chem. Phys. Lett.* **2004**, *394*, 257.
(16) Wang, Y.; Teitel, S.; Dellago, C. *J. Chem. Phys.* **2005**, *122*, 214722.
(17) Hoss, A.; Nold, M.; von Blanckenhagen, P.; Meyer, O. *Phys. Rev. B* **1992**, *45*, 8714.
(18) (a) Ocko, B. M.; Gibbs, D.; Huang, K. G.; Zehner, D. M.; Mochrie, S. G. *J. Phys. Rev. B* **1991**, *44*, 6429. (b) Mochrie, S. G. J.; Zehner, D. M.; Ocko, B. M.; Gibbs, D. *Phys. Rev. Lett.* **1990**, *64*, 2925.
(19) (a) Huang, K. G.; Gibbs, D.; Zehner, D. M.; Sandy, A. R.; Mochrie, S. G. J. *Phys. Rev. Lett.* **1990**, *65*, 3313. (b) Watson, G. M.; Gibbs, D.; Song, S.; Sandy, A. R.; Mochrie, S. G. J.; Zehner, D. M. *Phys. Rev. B* **1995**, *52*, 12329. (c) Carnevali, P.; Ercolessi, F.; Tosatti, E. *Phys. Rev. B* **1987**, *36*, 6701.
(20) Buffat, Ph.; Borel, J.-P. *Phys. Rev. A* **1976**, *13*, 2287.
(21) Pedemonte, L.; Bracco, G. *Surf. Sci.* **2002**, *513*, 308.
(22) Yang, H.-N.; Lu, T.-M.; Wang, G.-C. *Phys. Rev. Lett.* **1989**, *63*, 1621.
(23) Spiller, G. D. T. *Philos. Mag. A* **1982**, *46*, 535.
(24) Diao, J.; Gall, K.; Dunn, M. L. *Phys. Rev. B* **2004**, *70*, 1098.

NL051149H